Copolyureas formed by reaction injection moulding: correlations between chemical structure, thermal properties and microphase separation

Anthony J. Ryan, John L. Stanford* and Adrian J. Birch†
Polymer Science and Technology Group, Manchester Materials Science Centre, University of Manchester and UMIST, Grosvenor Street, Manchester M1 7HS, UK
(Received 20 April 1993)

Segmented copolyureas comprising soft segments based on a polyoxypropylene polyamine and hard segments based on 4,4'-diphenylmethane diisocyanate (MDI) reacting with either 3,5-diethyltoluenediamine (DETDA) or methylene-bis-2,6-diisopropylaniline (MDIPA) have been formed by reaction injection moulding (RIM). Novel RIM materials with MDI/DETDA hard segments and poly(dimethylsiloxane) soft segments have also been studied. RIM materials were characterized by d.s.c. and d.m.t.a. to obtain soft- and hard-segment glass transition temperatures, T_g^S and T_g^H, and the degree of microphase separation. Correlations between the chemical structure, thermal properties and microphase separation have been established using interaction parameters, χ, estimated from solubility parameters, and critical values of χ estimated from block copolymer theory. Hard-segment sequence length increases with hard-segment content, and values of T_g^H are shown to increase according to the Flory–Fox relation. The effects of process and thermal histories on microphase separation are interpreted with reference to a phase diagram.

(Keywords: reaction injection moulding; polyurea; microphase separation)

INTRODUCTION

The formation of copolyureas[1] from mixtures of aliphatic and aromatic amines reacting with aromatic isocyanates occurs via consecutive random-step polymerization reactions under the conditions prevalent in reaction injection moulding (RIM)[2]. The rates of reaction are such that RIM is the only way to form these engineering polymers[3]. With branched reactants[4,5], a combination of chemical gelation, spinodal decomposition-induced microphase separation[6] and vitrification, as liquid is converted rapidly to solid, effectively quenches the system to yield a mixture of reaction products comprising homopolymers, various AB-type block copolymers and free monomers[7]. This solid mixture possesses a non-equilibrium morphology[3,4,8] which arises from the direct competition between kinetic and thermodynamic changes occurring during the RIM process. Extensive experimental work has shown[3–6,9] that such a morphology comprises co-continuous, soft- and hard-segment microphases, and the degree of microphase separation depends on hard-segment content and thermal history. Further experimental evidence for these proposals is reported in this paper which directly supplements earlier work[3–9] by providing thermal property relations over a much wider composition range for non-linear copolyureas of various hard- and soft-segment structures.

EXPERIMENTAL

Reactants

The materials in this study were formed using three components: (i) a polyisocyanate, (ii) a polyether or polysiloxane polyamine and (iii) an aromatic diamine chain extender. The chemical structures of the various reactants used are shown in *Scheme 1*.

The polyisocyanate (**I**), Isonate M143 (Dow Chemical), is a uretonimine-modified version of 4,4'-diphenylmethane diisocyanate (MDI) and is a straw-coloured, low-viscosity liquid (0.02 Pa s at 25°C) with an equivalent weight of 143 ± 2 g mol^{-1} by isocyanate titration[10].

The polyether (**II**), Jeffamine T5000 (Texaco Chemical Company), is a polyoxypropylene triamine with a nominal molar mass of 5000 g mol^{-1} and an equivalent weight of 1900 g mol^{-1} ($-NH_2$) by potentiometric amine titration[11] and acetylation[12]. The polysiloxane (**III**), Q2-8075 (Dow Corning), is an amino-functionalized poly(dimethylsiloxane) (PDMS) with a nominal molar mass of 8300 g mol^{-1} and a primary amine equivalent weight of 2070 g mol^{-1}.

The aromatic diamines are an 80:20 mixture of the 2,4 and 2,6 isomers of 3,5-diethyltoluene diamine (DETDA) (**IV**) and methylene-bis-2,6-diisopropylaniline

* To whom correspondence should be addressed
† Present address: Dow Europe SA, CH-8810, Horgen, Switzerland

0032-3861/93/234874-08

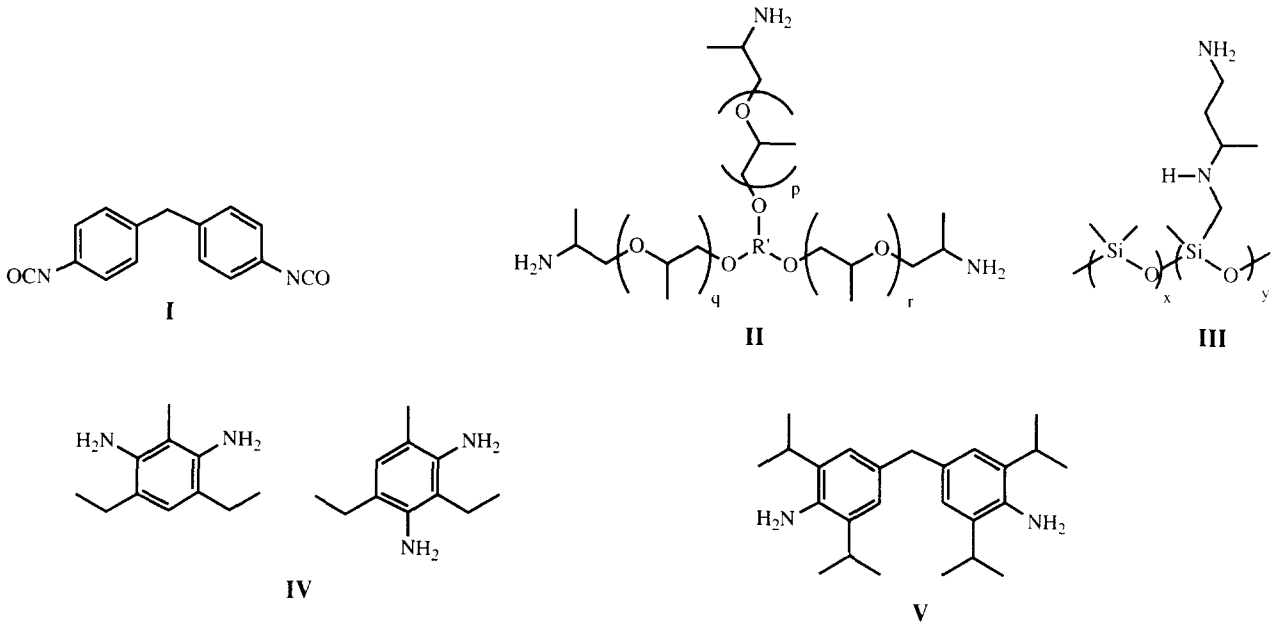

Scheme 1 Idealized reactant structures

Table 1 Formulations and processing data for RIM copolyureas

	UD30	UD40	UD50	UD60	UD70	UMD40	UMD50	UMD60	UMD70	USD50	USD70
M340[a]	237	219	202	194	189	111	103	98	95	200	188
T5000[a]	597	382	249	163	104	254	169	112	71	–	–
Q2-8075[a]	–	–	–	–	–	–	–	–	–	295	104
DETDA[a]	100	100	100	100	100	–	–	–	–	100	100
MDIPA[a]	–	–	–	–	–	100	100	100	100	–	–
Q_i (g s^{-1})	40.6	55.8	70.7	73.0	75.4	38.0	46.0	51.6	54.0	69.4	93.5
Q_p (g s^{-1})	119	123	122	98.8	81.2	121	121	111	97.4	121	101
μ_p (Pa s)	0.40	0.37	0.34	0.30	0.25	0.54	0.59	0.68	1.08	0.30	0.34
Re_p	393	431	468	477	519	294	268	223	132	529	426

[a] The numbers in the table represent the parts by weight of reactants used in formulations

(MDIPA) (V). Both chain extenders (Lonza AG) were thoroughly characterized by combustion analysis and n.m.r. spectroscopy prior to use[13]. All of the reactants (I)–(V) were used as received without further purification.

Reaction injection moulding (RIM)

Polyureas were moulded as rectangular plaques (150 × 400 × 3 mm) using in-house RIM equipment that has been described in detail elsewhere[14]. The formulations and processing data are given in *Table 1*, where Q_p and Q_i are the machine throughputs used, respectively, for the polyamine and the polyisocyanate reactant streams, μ_p and Re_p are the viscosity and the Reynolds number of the polyamine blend. Initial reactant temperatures of 35 and 40°C for the polyisocyanate and polyamine blend, respectively, and a mould temperature of 115°C were used throughout. The stoichiometric ratio of isocyanate to total amine groups used was 1.03. Good mixing was achieved and the materials showed no visible striations or gel-lines. Plaques were removed from the mould after a period of at least 1 min. The copolyureas produced are designated using a code (see the top row in *Table 1*) comprising the soft- and hard-segment type, T5000/DETDA (UD), T5000/MDIPA (UMD) or Q2-8075/DETDA (USD), and the weight percentage of hard segment. For example, UD50 comprises 50% by weight of MDI/DETDA hard segment and a polyether soft segment.

Differential scanning calorimetry (d.s.c.)

D.s.c. studies were performed on a DuPont 990 Thermal Analyser fitted with a DuPont 910 cell base, equipped with a 990 d.s.c. cell. Samples (12–18 mg) and an inert reference material, 10 mesh glass beads (13 mg), were encapsulated in aluminium pans and cooled rapidly to −120°C in the cell. The sample and reference were subjected to a 20°C min^{-1} ramp rate in static air to 350°C. The glass transition temperatures were obtained from the d.s.c. trace at the intersection of the tangents drawn to the onset baseline and the endothermic slope.

The degrees of phase separation for the copolymers studied were obtained using the method of Camberlin and Pascault[15]; thus, the heat capacity change ΔC_p^S at the soft-segment glass transition, T_g^S, was measured and compared with ΔC_p^{S0} of the pure soft-segment material. Knowing the hard-segment fraction of the material, the phase separation ratio (*PSR*) was established as described previously[4,5,13,14].

Dynamic mechanical thermal analysis (d.m.t.a.)

D.m.t.a. data were obtained in the temperature range −100 to 300°C using a Polymer Laboratories apparatus operating at a frequency of 1 Hz and a heating rate of 5°C min^{-1}. A double cantilever bending geometry was used for beam samples (3 × 10 × 45 mm) to obtain dynamic flexural moduli and mechanical damping as functions of temperature.

RESULTS AND DISCUSSION

Processing

Materials UD40–UD70 based on DETDA chain extender were successfully produced as solid plaques ranging from ductile to brittle plastics. All materials were visually homogeneous with dark amber colouration and translucent appearance. Post-mixing solidification time was less than 1 s in all cases, and demoulding of plaques was easily achieved. However, UD30 materials were observed to contain 'knit lines'[2], which occurred due to the extremely rapid gelation before complete mould filling was achieved. UD70 materials were found to have low green strength, with some plaques cracking within the mould cavity during mould opening. All materials were stored at room temperature until required for testing and some plaques were post-cured immediately after demoulding at 200°C for 1 h.

Materials UMD50–UMD70 based on MDIPA chain extender were successfully produced as visually homogeneous, translucent plaques with light amber colouration. However, air entrainment around the edges of plaques was apparent. Solidification times were again less than 1 s and demoulding was relatively easy. UMD70 materials were found to be extremely brittle, with the majority of plaques cracking while still in the mould. This brittleness was observed to diminish substantially within a day of demoulding. Samples were unsuccessfully post-cured at 200°C for 1 h. Air trapped during mould filling expanded (blowing) during post-cure, causing distortion to all samples. The post-cure temperature was therefore reduced until blowing was undetected. Hence UMD materials were post-cured at 150°C for 1 h. After post-curing, all UMD materials were observed to become lighter in colour.

The processing of RIM materials based on the siloxane polyamine and DETDA chain extender was relatively unsuccessful. Continuous recirculation of the reactants and holding tank agitation were required to stop the DETDA and Q2-8075 mixture separating. The USD50 system was observed to 'extrude' from the mix-head as a cream-coloured, friable solid and no attempt was made to mould this material. The USD70 system was observed to leave the mix-head as a highly viscous fluid which solidified within a distance of ~10 cm from the nozzle exit. Two plaques of this cream-coloured opaque solid were successfully produced, one of which was post-cured immediately after demoulding at 200°C for 1 h. USD70 materials were extremely brittle and required gentle handling. Testing of USD70 was performed using d.s.c. and d.m.t.a.

Microphase separation

In an attempt to predict the phase behaviour of the formulations used in this study, values of the hard-segment/soft-segment interaction parameter, χ_{HS}, have been calculated from solubility parameters, ∂, and compared with the critical interaction parameter, χ_c, estimated from the data of Liebler[16] and Benoit and Hadziannou[17]. Idealized structures have been assumed for the soft and hard segments to allow estimation of ∂_H, ∂_S, N_H and N_S. The first assumption is that hard segments are based on pure MDI. Other assumptions are that the $(AB)_n$ structure of the copolymer is linear and N_S is the product of two arms of the polyamine, and that the reaction is assumed to proceed to completion so that N_H may be calculated from a knowledge of N_S and f.

Values of χ_{HS}, normalized to the soft segment, have been calculated according to the Hildebrand–Scratchard equation[18,19] and are presented in *Table 2*, along with values for the reference volume (mass of repeat unit divided by density), V_S[20], and the solubility parameters of the hard and soft segments, ∂_H and ∂_S, calculated by Ryan *et al.*[21]. Furthermore, values of ∂_S for T5000 and Q2-8075 have been approximated to those of POP and PDMS, respectively. Values of χ_c have been estimated by the spinodal product $(\chi N)_S$ at each soft-segment weight fraction used in this study. Values of χ_{HS} are given in *Table 2* and values of the ratio χ_{HS}/χ_c are presented in *Table 3*.

The application of the Liebler theory predicts that all of the RIM systems studied should microphase separate since, in all cases, $\chi_{HS} > \chi_c$, i.e. the values of the ratio χ_{HS}/χ_c given in *Table 3* exceed unity. Furthermore, it has been suggested[5] that the driving force for microphase separation is related to the magnitude of the ratio. Hence the values of this ratio presented in *Table 3* predict that the degree of microphase separation should increase with increasing hard-segment content for each series of materials, and that the degree of microphase separation should be in the order USD > UD > UMD.

Differential scanning calorimetry

Figure 1 shows sub-ambient d.s.c. traces for non-post-cured UD materials and for a model network based on M340/T5000. Derived d.s.c. data for the copolyurea (PUr) materials are presented in *Table 3*. The value of T_g^S for the PUrs containing T5000 soft-segment oligomer shows only a slight increase with increasing hard-segment content, indicating that only a low concentration of the hard segment is dissolved in the soft-segment phase. The effect of hard-segment structure on T_g^S is relatively small; at equivalent hard-segment content, T_g^S is approximately 1 to 2°C higher for materials containing MDIPA chain extender as opposed to DETDA. Replacing T5000 with the siloxane-based soft-segment oligomer decreases T_g^S for USDP70NP to −111°C. T_g^S for phenyl isocyanate-capped Q2-8075 was found to be −119°C. This difference of 8°C arises from restriction in mobility imposed on the soft-segment units within the USD70NP network as a result of chain ends being fixed. No further thermal changes were observed by d.s.c. except for the onset of thermal oxidative degradation (250–300°C). Comparison

Table 2 Calculated values of χ_{HS} at 298 K normalized to the soft-segment repeat unit

Material	V_s ($cm^3\ mol^{-1}$)	∂_H ($cal^{1/2}\ cm^{-3/2}$)	∂_S ($cal^{1/2}\ cm^{-3/2}$)	χ_{HS}
UD	55	12.4	8.1	1.72
UMD	55	10.6	8.1	0.58
USD	76	12.4	7.5	3.08

Table 3 Effects of copolyurea composition on χ_{HS}/χ_c, T_g^S and *PSR*

Copolyurea	f^a	N_S	N_H	$\chi_c (N_H+N_S)^b$	χ_c	χ_{HS}/χ_c	$T_g^{S\,c}$ (°C)	*PSR*
UD30	0.64	65.5	36.9	17.0	0.17	10.1	−61	0.63
UD40	0.55	65.5	55.8	15.0	0.14	12.3	−60	0.67
UD50	0.45	65.5	78.6	15.5	0.11	15.6	−60	0.71
UD60	0.36	65.5	116.5	17.0	0.09	19.1	−59	0.71
UD70	0.26	65.5	186.5	25.0	0.09	19.1	−59	0.68
UMD40	0.55	65.5	52.4	15.0	0.14	4.1	−60	0.84
UMD50	0.45	65.5	78.6	15.5	0.11	5.3	−59	0.60
UMD60	0.36	65.5	116.5	17.0	0.09	6.4	−59	0.44
UMD70	0.26	65.5	186.5	25.0	0.09	6.4	−59	0.31
USD50	0.50	55.9	55.9	15.0	0.13	23.7	–	–
USD70	0.27	55.9	151.3	24.0	0.12	26.6	−113	0.85

[a] Weight fraction of polyether
[b] Estimated from the phase diagram in ref. 16
[c] $T_g^S = -61$°C for the separately-synthesized soft segment M340/T5000: $T_g^S = -119$°C for the functionalized PDMS (Q2-8075)

Table 4 The effect of copolyurea composition on thermal properties derived from d.m.t.a.

Copolyurea	T_g^S (°C)	tan δ (T_g^S)	T_g^H (°C)	tan δ (T_g^H)	N_n	$E'(-30°C)/E'(65°C)$	$E'(65°C)/E'(160°C)$
UD30	−40	0.20	220[a]	0.38[a]	3.8	6.7	1.6
UD40	−40	0.15	236	0.43	5.9	3.7	1.5
UD50	−39	0.11	233	0.42	8.9	3.5	1.4
UD60	−39	0.09	235	0.51	13.3	2.5	1.4
UD70	−40	0.07	247	0.61	20.7	1.9	1.3
UMD40	−41	0.22	[b]	[b]	4.1	8.9	2.8
UMD50	−35	0.13	171	0.13	6.2	6.9	2.2
UMD60	−35	0.07	179	0.15	9.3	5.0	2.2
UMD70	−35	0.05	184	0.17	14.4	3.0	2.6
USD70	−106	0.06	241	0.63	21.7	1.5	1.2

[a] Observed only as a shoulder in tan δ *versus* temperature curves
[b] Not detected

of T_g^S data in *Table 4* for as-moulded and annealed materials shows that post-curing has little effect on the location of T_g^S.

Values of *PSR* for as-moulded and annealed PUr are presented in *Table 3* as the ratio of the heat capacity change of PUr at T_g^S compared to that of the pure soft-segment model, normalized for sample mass. The value of *PSR* is a measure of the amount of soft segment which contributes to heat capacity at T_g^S and therefore does not include soft segment trapped either in the hard segment or involved in the interphase regions.

Figure 2a shows plots of *PSR versus* hard-segment content for UD and USD materials. The experimental values of *PSR* show a slight deviation towards phase mixing with decreasing hard-segment content. The theoretical predictions from solubility arguments indicate that these materials should be completely microphase separated. However, the theoretical predictions are based on equilibrium conditions which are not achieved in these rapidly-formed copolymers. At low hard-segment contents, solidification occurs by chemical gelation of the soft-segment network (premature gelation was observed for UD30) which is more rapid than the phase separation process and, consequently, short hard-segment sequences with low T_g^H are formed. At higher hard-segment contents, higher average sequence lengths of hard-segment blocks with higher T_g^H are achieved, leading to an increase in

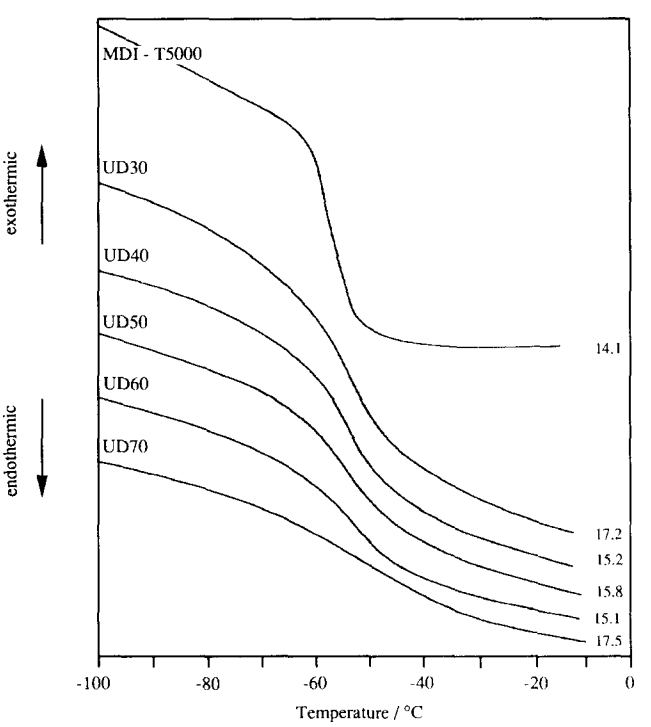

Figure 1 D.s.c. traces for the UD series of materials. Numbers on right-hand side of curves are sample masses (mg). Also included is the d.s.c. trace for isolated MDI/T5000 soft segment

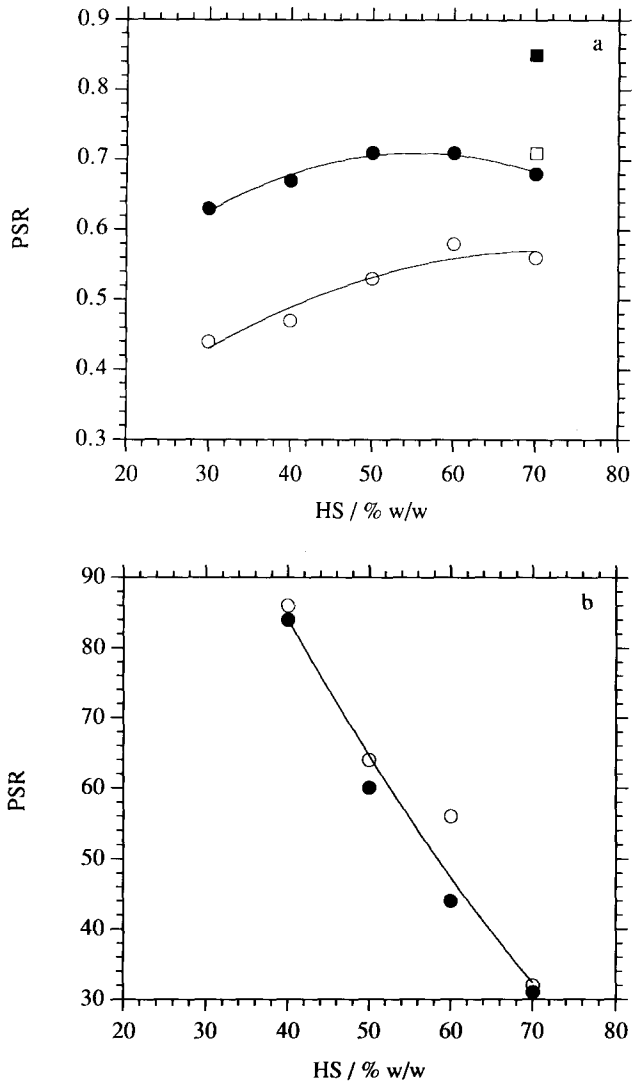

Figure 2 Variation of *PSR* with hard-segment content for: (a) USD and UD series: (○) UD as-moulded, (●) UD annealed for 1 h at 200°C, (■) USD as-moulded, (□) USD annealed for 1 h at 200°C; (b) UMD series: (○) as-moulded, (●) annealed for 1 h at 150°C

the driving force for microphase separation. Complete phase separation does not occur since the process is arrested by solidification as the hard segment vitrifies. During polymerization the hard-segment sequence length builds up to such a level that its T_g^H exceeds the temperature within the mould (T_{RIM}), even allowing for the reaction exotherm. Since $T_g^H > T_{RIM}$, vitrification occurs instantaneously. As-prepared USD70 has a *PSR* of 0.71, which indicates good phase separation. Theoretical predictions indicate that the driving force for phase separation is greater than that for UD70. The USD material is opaque with very poor physical strength and the high degree of phase separation is associated with poor phase connectivity; that is, the hard and soft segments are not completely covalently bonded to each other. Premature phase separation is more likely to occur in this system due to the inherent incompatibility of the siloxane polyamine with both M340 and DETDA.

Figure 2b shows a plot of *PSR versus* hard-segment content for UMD PUr. The trends in the experimental values of *PSR* (*Table 3*) are towards phase mixing at higher hard-segment contents. Theoretical predictions (*Table 3*) indicated that these materials should have an increased driving force towards phase separation with increases in hard-segment content. This is not observed and the difference between theory and experiment highlights the difficulties in accurately predicting the phase behaviour of these complex non-equilibrium PUr systems, using simple thermodynamic arguments. An equivalent RIM PUU system has been studied[22] and a similar decrease from 0.80 to 0.45 was observed in *PSR* as the hard-segment content increases from 0.52 to 0.65. It should be noted that the value of χ_{HS}/χ_c for the PUr materials studied here indicate that UD systems should be more phase separated than UMD systems, and in general this is observed. Annealing UMD materials has no significant effect on the degree of phase separation within the experimental error of the d.s.c. measurements.

Dynamic mechanical thermal analysis

In general, two major transitions are observed for the PUr materials studied ascribed to the soft- and hard-segment glass transitions at temperatures T_g^S and T_g^H, respectively. *Figure 3* shows typical storage modulus (E') and damping (tan ∂) *versus* temperature data for the 70% hard-segment materials and derived DMTA data are shown in *Table 4*. The existence of two transitions implies that all the materials are microphase-separated block copolymers. T_g^S occurs at ≈ -40°C for T5000 soft segment and ≈ -100°C for the siloxane soft segment. The values of T_g^S observed by d.m.t.a. are consistently higher than those observed by d.s.c. because of intrinsic differences in the techniques. D.m.t.a. measurements are transitional peaks, whereas in d.s.c., transitional behaviour is determined from a non-mechanical technique and values of T_g^S relate to onset temperatures.

The value of T_g^S is relatively insensitive to the hard-segment content as shown in *Table 4*, and as would be expected from composition considerations, the maximum value of tan ∂ increases as the volume fraction of soft segment increases. The UD series have $T_g^S \approx -40$°C compared with -35°C for the UMD series which is consistent with the thermodynamic calculations

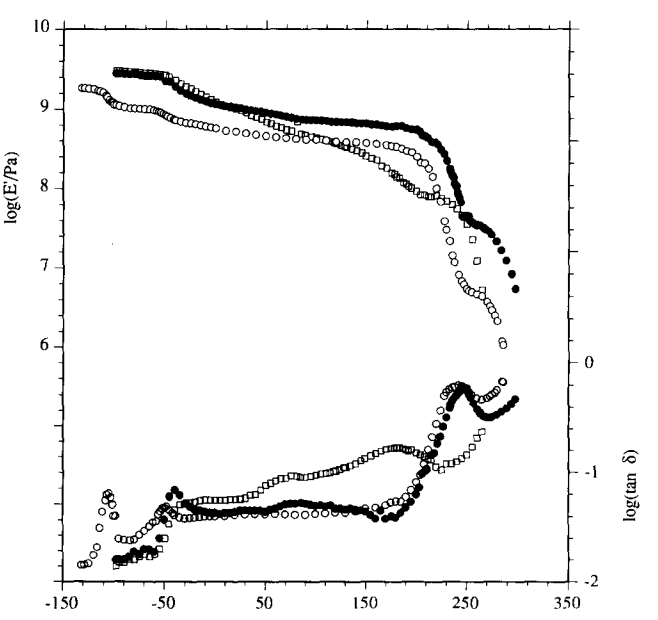

Figure 3 Dynamic flexural modulus (E') and mechanical damping (tan ∂) at 1 Hz *versus* temperature for 70% w/w hard-segment copolyureas: (●) UD; (□) UMD; (○) USD

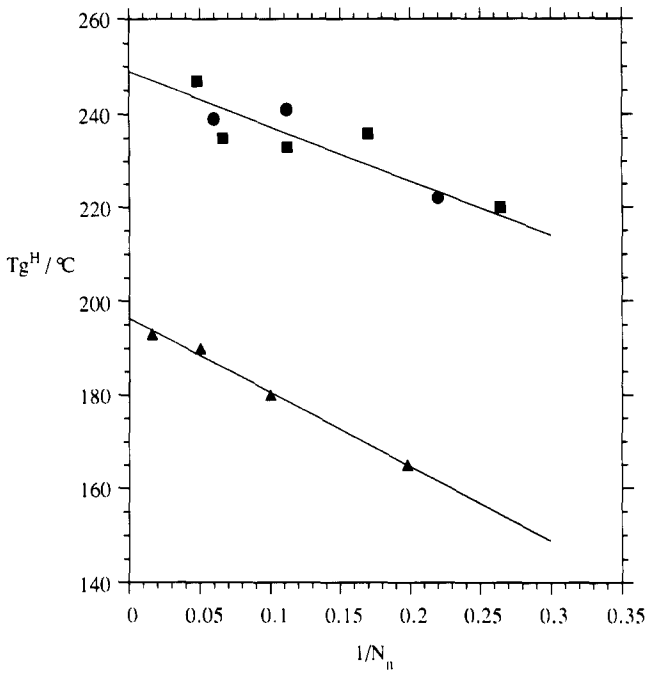

Figure 4 Glass transition temperatures *versus* the reciprocal hard-segment sequence length ($1/N_n$) for UD RIM copolyureas; present work (■), ref. 4 (●) and specially synthesized UMD hard-segment oligomers (▲). The lines are least-squares fits according to the Flory–Fox equation

and *PSR* data in *Table 3*. The materials based on PDMS have distinctly different low-temperature dynamic behaviour with two pronounced transitions; the lower transition is T_g^S at $-106°C$ and the higher transition at $-48°C$ is probably associated with the melting of PDMS crystals[20].

In all materials the modulus below T_g^S is ≈ 3 GPa and the magnitude of the sharp decrease at T_g^S depends on the hard-segment content and the chemical structure. The magnitude of the often quoted[2] ratio of moduli at -30 and 65°C is dominated by the modulus change associated with T_g^S, phase mixing and in the case of UMD the close proximity of T_g^S to $-30°C$. The effect of segmental mixing may be observed in the variation of the ratio with chemical structure, that is, UMD > UD > USD.

The tan ∂ curves show a broad transition between 50 and 150°C which is associated with breakdown of hydrogen bonding between hard-segment polyurea (amide) groups and soft-segment polyether (oxygen). The materials with the greatest segmental mixing have the most intense tan ∂ peaks; see for example *Figure 3*, which shows a sharp transition for UMD70 and virtually no change in tan ∂ for USD70. The temperature sensitivity of the modulus in this temperature interval is quantified by the ratio of moduli at 65 and 160°C shown in *Table 4*. UD and USD are well microphase-separated and the modulus ratios are close to one whereas the more microphase-mixed UMD materials have values between two and three.

T_g^H occurs between 160 and 250°C, depending on hard-segment structure and content. Some difficulties were encountered in assigning values of T_g^H at low hard-segment content due to the onset of thermal-oxidative degradation of the polymer which occurs in the temperature range close to T_g^H. For the UD series, the maximum value of tan ∂ increases with the volume fraction of the hard segment because the *PSR* is high and essentially constant. In contrast, the magnitude of tan ∂ associated with T_g^H for the UMD materials is very low and essentially independent of the hard-segment content since the effects on damping of increasing hard-segment content is offset by decreases in *PSR*. USD70, which has the highest measured value of *PSR*, also has a very sharp T_g^H peak.

Dependence of T_g^H *on hard-segment sequence length*

The T_g^H data for UD and USD indicate that the location of T_g^H is due to 'pure', well-segregated segments and are amenable to interpretation using the Flory–Fox equation[23]. Thus

$$T_g = T_g^\infty + \frac{B}{N_n}$$

where T_g^∞ and B are polymer specific constants, and in this case N_n is the number-average hard-segment sequence length calculated from stoichiometry and presented in *Table 4*. The data presented in *Figure 4* for the UD series follow the prediction and extrapolate to $T_g^\infty = 249 \pm 2°C$. The fact that the two sets of data follow the prediction of Flory and Fox is further evidence of the existence of the glass transition in polyureas formed from DETDA and MDI.

In contrast, the T_g^H data for the UMD series do not correlate with the predictions of Flory–Fox, and this is due to the low degree of microphase separation in these copolyureas. However, to further investigate the T_g^H dependence on sequence length of the UMD materials, some subsidiary experiments were carried out in which model hard-segment sequences were synthesized, in isolation, using MDIPA and MDI in various stoichiometric ratios in NMP solution[13]. The mechanical damping–temperature behaviour of the isolated hard segment was investigated by the supported braid technique[13] to give T_g^H values and these are plotted in *Figure 4*. Again the data follow the predictions of Flory–Fox and extrapolate to $T_g^\infty = 197 \pm 2°C$. The differences in T_g^∞ and the slopes of the lines, B, may be rationalized in terms of the intrinsic flexibilities of the polymer backbones and the densities of urea groups, and thus hydrogen bonding[3]. The DETDA polyurea backbone is intrinsically stiffer than that of the MDIPA polyurea and its increased urea-group density compounds this stiffness giving a higher value of T_g^∞ and a smaller slope, B.

Effects of process and thermal history on microphase separation

The *PSR* values determined from d.s.c. and the d.m.t.a. data have shown both UD and UMD PUr to be partially phase-separated copolymers. It is also evident that on annealing, *PSR* values for UD increase while little significant change is observed for UMD materials. The explanation for these observed differences in the degree of phase separation from theory is not due simply to the complex non-equilibrium nature of these non-ideal, $(AB)_n$-type segmented block copolymers. In fact, the thermodynamics and phase behaviour of the bulk polymerization are more like those of a mixture or blend. Comparison of the calculated equilibrium values of χ_{HS} ($\gg 0.5$, see *Table 2*) and χ_{HS}/χ_c ($\gg 1$, see *Table 3*) indicates that both UD and UMD PUr have a large driving force for both phase separation of a mixture and microphase

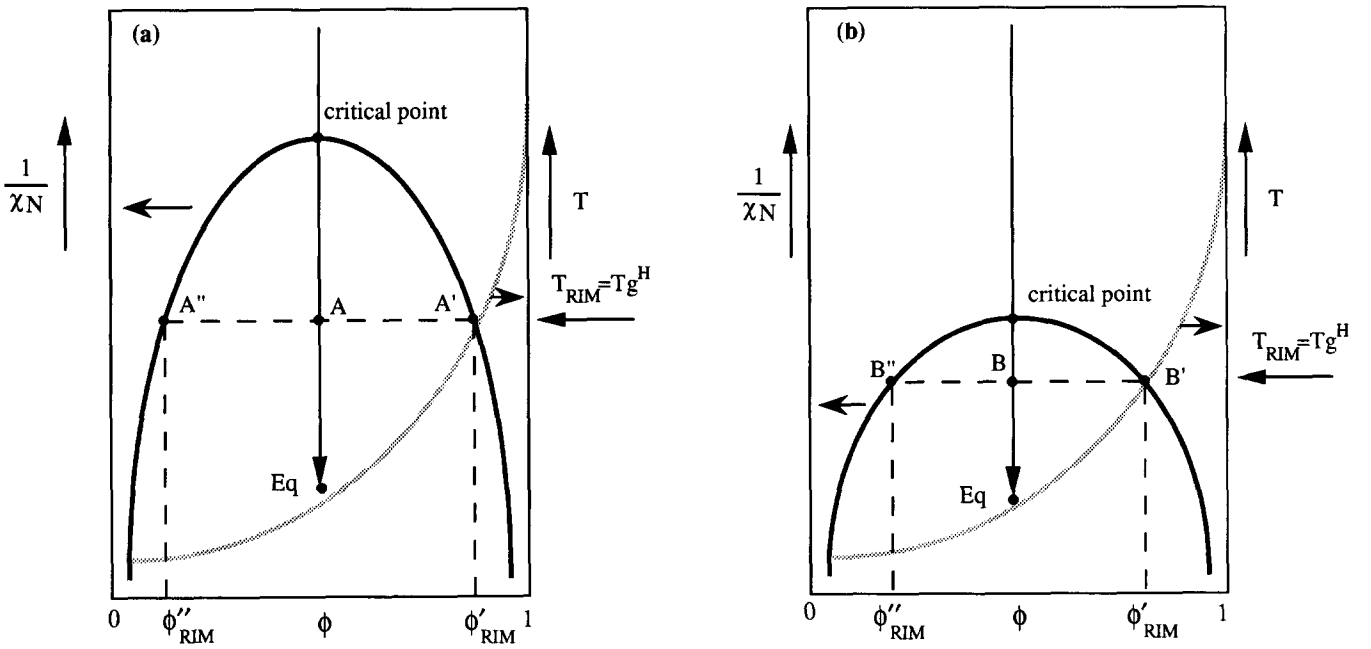

Figure 5 Schematic representations of the phase diagram coexistence curves (solid curves), superimposed with schematic T_g *versus* composition curves (dotted curves) for: (a) UD material; (b) UMD material

separation of a block copolymer, respectively. As described previously[5,6], the reacting mixture, which ultimately forms a copolyurea, phase separates by a spinodal decomposition process due to the rapid increase in N $(=N_H+N_S)$ during the RIM reaction.

Figures 5a and *5b* show schematic representations of the phase diagrams for UD and UMD materials. To aid discussion, the coexistence curves have been positioned symmetrically and the process is assumed to be isothermal, although neither of these assumptions is realistic. The coexistence curve can be defined in terms of either T or $1/N$ (on the ordinate), but in this simplified discussion only $1/N$ is used since the RIM process is assumed to be isothermal. In such phase diagrams, the interphase region is considered to be infinitesimally small. Values of the ratio χ_{HS}/χ_c at 25°C (see *Table 3*) show that the driving force for phase separation is three times greater for UD materials than for UMD. Consequently, the coexistence curve for UD materials (*Figure 5a*) has a higher critical point than for UMD PUr (*Figure 5b*), so that the equilibrium position, Eq, of UD at RIM processing temperatures and final values of N lies deeper in the unstable region of the phase diagram compared to that of UMD. Superimposed on each phase diagram is a T_g *versus* composition curve for the homogeneous mixtures assuming complete reaction. In the case of UD (*Figure 5a*), polymerization proceeds rapidly and acts as a large thermodynamic quench, taking the reaction mixture into the unstable region (represented by the vertical arrow). Large values of N are quickly achieved, leading to the two-phase equilibrium position (Eq). The phase separation process lags behind the reaction and is ultimately arrested by the vitrification of the phase richer in hard segment, which attains a composition with T_g^H equivalent to the in-mould reaction temperature, T_{RIM}. This occurs at position A′ which is known as the Berghmans point[24] and no further separation is possible. Thus, the values ϕ'_{RIM} and ϕ''_{RIM} define the composition of the final RIM material, and clearly the composition is far from equilibrium. For UMD materials (*Figure 5b*), the phase separation process is similar, but the equilibrium position, Eq, being closer to the 'critical point', is not so deep in the unstable region of the phase diagram. The Berghman point, B′, is lower than in UD since T_g^H is 50°C lower. Again at B′, vitrification occurs so that compositions ϕ'_{RIM} and ϕ''_{RIM} are obtained. It is clear that such compositions are less pure in either soft or hard segment than those obtained at the Bergman point for UD, and this conclusion is in accord with the experimental values of T_g^S, T_g^H and *PSR*.

Annealing UD materials at 200°C for 1 h increases *PSR*. For example, in the case of UD40, annealing increases *PSR* from 0.47 to 0.67. The annealing temperature of 200°C is below the glass transition of the hard-segment-rich phase. The final compositions are defined by ϕ'_{RIM} and ϕ''_{RIM} in the phase diagram. During annealing, the hard-segment-rich phase with composition ϕ'_{RIM} therefore remains in the glassy state and no further phase separation, increasing ϕ'_{RIM}, occurs. As previously stated, the phase diagram assumes an infinitesimally small interphase. However, an interphase must exist in which there is a gradual change in composition between the two dominant phases ϕ'_{RIM} and ϕ''_{RIM}, and this is illustrated in *Figure 6*, a schematic representation of the development of the composition profile for a UD material as it phase separates during the RIM process. The horizontal dashed line represents the mean composition of the system, and this may be regarded as the initial mother phase created by impingement mixing. As polymerization occurs, N increases and the system undergoes spinodal decomposition leading to phase separation of a mixture; the dominant wavelength of the structure so formed is set by the radius of gyration of the soft-segment chains. (The first species to be formed are MDI-tipped soft-segment oligomers and these effectively act as a surfactant, stabilizing the size-scale of the subsequent phase growth). On annealing, the material has limited Brownian motion and chain segments diffuse within the limits of their covalent bonds. Diffusion against the composition gradient results in sharpening of the

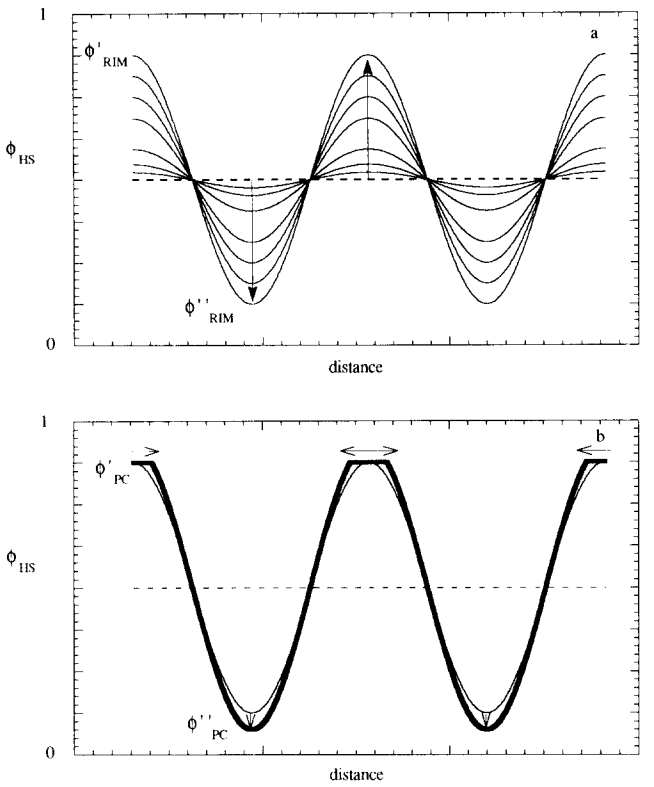

Figure 6 Schematic representations of the compositional profiles of a UD material formed by RIM: (a) developed during RIM from phase separation by a spinodal decomposition process; (b) developed during annealing below T_g^H

interphase and an increase in purity of the soft-segment-rich phase to composition ϕ''_{PC}, and a coarsening of the hard-segment-rich phase without a change in composition, so that $\phi'_{PC} = \phi'_{RIM}$. This process is shown schematically in *Figure 6b*. Values of T_g^H for UD materials are not affected by annealing (see Figure 5 in ref. 9) but a reduction in mechanical damping between T_g^S and T_g^H and intensification of the tan δ peak associated with T_g^H indicate that interphase demixing has occurred.

SUMMARY AND CONCLUSIONS

Novel RIM copolyureas (USD series) with poly(dimethylsiloxane) soft segments and MDI/DETDA hard segments, are more microphase separated than copolyureas (UD and UMD series) comprising polyether soft segments and, respectively, either MDI/DETDA or MDI/MDIPA hard segments according to d.s.c. and d.m.t.a. data. Correlations between the chemical structure, thermal properties and microphase separation have been established using interaction parameters, χ_{HS}, estimated from solubility parameters and critical values of χ_c estimated from block copolymer theory[16,17]. For the polyether-based materials (UD and UMD series), T_g^S is $\approx -60°C$ and is independent of hard-segment structure or content. The *PSR* associated with T_g^S is, however, sensitive to both hard-segment structure and annealing. Values of T_g^H are shown to depend on hard-segment sequence length according to the Flory–Fox relation. The effects of process and thermal history on microphase separation have been interpreted with reference to a phase diagram.

The reaction injection moulding process involves the conversion of a mixture of monomers into a block copolymer. The polymerization reaction competes with phase separation of the complex mixture to form a solid product with a non-equilibrium morphology. Generally, the hard-segment polyurea forms rapidly and this initiates phase separation, and the size-scale of the incipient microphase is set by the initial block copolymer which is formed by the rapid isocyanate end-capping of the polyamine. The concentration profile grows until the T_g of the urea-rich phase coincides with the polymerization temperature (mould temperature and reaction exotherm). Vitrification then locks-in the composition profile with urea-rich and polyether-rich microphases as illustrated in *Figures 5* and *6*. Owing to the high T_g of the aromatic urea, the quenched composition profile is relatively weak, that is, sinusoidal in shape rather than square-wave. The polyether phase contains significant proportions of polyurea, and *vice versa*. Consequently, the T_g of the polyether is broad and shifted from that of the pure soft segment. Annealing will allow some improvement in morphology but, as was observed, annealing below the T_g of the hard-segment microphase will only purify the polyether microphase.

ACKNOWLEDGEMENTS

The authors wish to acknowledge the kind donation of reactants from DOW Benelux NV, Texaco Chemicals and LONZA AG. A. J. B. was supported by an SERC Studentship.

REFERENCES

1 Ryan, A. J. and Stanford, J. L. in 'Comprehensive Polymer Science' (Eds G. Allen and J. C. Bevington), Vol. 5, Pergamon Press, Oxford, 1988, Ch. 25, p. 427
2 Macosko, C. W. 'Fundamentals of Reaction Injection Moulding', Hanser, Munich, 1989
3 Stanford, J. L., Wilkinson, A. N., Lee, D.-K. and Ryan, A. J. *Plast. Rubber Proc. Appl.* 1990, **13**, 111
4 Ryan, A. J., Stanford, J. L. and Wilkinson, A. N. *Polym. Bull.* 1988, **18**, 517
5 Ryan, A. J., Stanford, J. L. and Still, R. H. *Plast. Rubber Proc. Appl.* 1990, **13**, 99
6 Ryan, A. J. *Polymer* 1990, **31**, 707
7 Willkomm, W. R. *PhD Thesis* University of Minnesota, 1990
8 Willkomm, W. R., Chen, Z. S., Macosko, C. W., Gobran, D. H. and Thomas, E. L. *Polym. Eng. Sci.* 1988, **28**, 888
9 Birch, A. J., Stanford, J. L. and Ryan, A. J. *Polym. Bull.* 1989, **22**, 629
10 ASTM D1638M
11 Texaco Chemical Company. Analysis Method No. ST-5.35-85, 1985
12 Sorrenson, W. R. and Campbell, T. W. 'Preparative Methods in Polymer Chemistry', Wiley Interscience, New York, 1981
13 Birch, A. J. *PhD Thesis* University of Manchester, UK, 1991
14 Wilkinson, A. N. *PhD Thesis* University of Manchester, 1990
15 Camberlin, Y. and Pascault, J. P. *J. Polym. Sci., Polym. Chem. Edn* 1983, **27**, 415
16 Leibler, L. *Macromolecules* 1980, **13**, 1602
17 Benoit, H. and Hadziannou, G. *Macromolecules* 1988, **21**, 1449
18 Scratchard, G. *Chem. Rev.* 1931, **8**, 321
19 Hildebrand, J. H. and Scott, R. L. 'The Solubility of Non-Electrolytes', 3rd Edn, Rhinehold, New York, 1950
20 Van Krevelen, D. W. 'Properties of Polymers: Correlations with Chemical Structure' 3rd Edn, Elsevier, Amsterdam, 1991
21 Ryan, A. J., Stanford, J. L. and Still, R. H. *Polym. Commun.* 1988, **29**, 196
22 Ryan, A. J., Stanford, J. L. and Still, R. H. *Polymer* 1991, **32**, 1427
23 Flory, P. J. and Fox, P. *J. Appl. Phys.* 1950, **21**, 581
24 Callister, S., Keller, A. and Hikmet, R. M. *Makromol. Chem., Makromol. Symp.* 1990, **39**, 19